
Factorized Inference in Deep Markov Models for Incomplete Multimodal Time Series

Zhi-Xuan Tan¹, Harold Soh², Desmond C. Ong¹

¹A*STAR AI Initiative, Agency for Science, Technology and Research, Singapore

²Department of Computer Science, National University of Singapore

xuan@mit.edu, harold@comp.nus.edu.sg, desmond.c.ong@gmail.com

Abstract

Integrating deep learning with latent state space models has the potential to yield temporal models that are powerful, yet tractable and interpretable. Unfortunately, current models are not designed to handle missing data or multiple data modalities, which are both prevalent in real-world data. In this work, we introduce a factorized inference method for Multimodal Deep Markov Models (MDMMs), allowing us to filter and smooth in the presence of missing data, while also performing uncertainty-aware multimodal fusion. We derive this method by factorizing the posterior $p(z|x)$ for non-linear state space models, and develop a *variational backward-forward algorithm* for inference. Because our method handles incompleteness over both time and modalities, it is capable of interpolation, extrapolation, conditional generation, and label prediction in multimodal time series. We demonstrate these capabilities on both synthetic and real-world multimodal data under high levels of data deletion. Our method performs well even with more than 50% missing data, and outperforms existing deep approaches to inference in latent time series.

1 Introduction

Virtually all sensory data that humans and autonomous systems receive can be thought of as multimodal time series—multiple sensors each provide streams of information about the surrounding environment, and intelligent systems have to integrate these information streams to form a coherent yet dynamic model of the world. These time series are often asynchronously or irregularly sampled, with many time-points having missing or incomplete data. Classical time series algorithms, such as the Kalman filter, are robust to such incompleteness: they are able to infer the state of the world, but only in linear regimes [1]. On the other hand, human intelligence is robust *and* complex: we infer complex quantities with *nonlinear dynamics*, even from incomplete temporal observations of multiple modalities—for example, intended motion from both eye gaze and arm movements [2], or desires and emotions from actions, facial expressions, speech, and language [3, 4].

There has been a proliferation of attempts to bridge this gap and learn nonlinear dynamics by integrating deep learning with traditional probabilistic approaches such as Hidden Markov Models (HMMs) and latent dynamical systems. Most approaches do this by adding random latent variables to each time step in an RNN [5, 6, 7, 8]. Other authors begin with latent sequence models as a basis, then develop deep parameterizations and inference techniques for these models [9, 10, 11, 12, 13, 14, 15]. Most relevant to our work are the Deep Markov Models (DMMs) proposed by Krishnan, Uri, and Sontag [9], a generalization of HMMs and Gaussian State Space Models where the transition and emission distributions are parameterized by deep networks.

Unfortunately, none of the approaches thus far are designed to handle inference with both missing data and multiple modalities. Instead, most approaches rely upon RNN inference networks [9, 12, 16], which can only handle missing data using ad-hoc approaches such as zero-masking [17], update-

skipping [9], temporal gating mechanisms [18, 16], or providing time stamps as inputs [15], none of which have intuitive probabilistic interpretations. For example, Che *et al.* extend DMMs to handle time series sampled at different rates by learning temporal gates, but do not handle arbitrary missingness [16], while Chen *et al.* learn neural ordinary differential equations that allow modelling of irregularly sampled data, but still rely on black-box RNNs with time-stamp concatenation for inference [15]. Of the approaches that do not rely on RNNs, Fraccaro *et al.* handle missing data by assuming linear latent dynamics [19], while Johnson *et al.* [11] and Lin *et al.* [14] use hybrid message passing inference that is theoretically capable of marginalizing out missing data. However, these methods are unable to learn nonlinear transition dynamics, nor do they handle multiple modalities.

We address these limitations—the inability to handle missing data, over multiple modalities, and with nonlinear dynamics—by introducing a multimodal generalization of Deep Markov Models, as well as a factorized inference method for such models that handles missing time points and modalities by design. Our method allows for both filtering and smoothing given incomplete time series, while also performing uncertainty-aware multimodal fusion *a la* the Multimodal Variational Autoencoder (MVAE) [20]. Because our method handles incompleteness over both time and modalities, it is capable of interpolation, forward extrapolation, backward extrapolation, conditional generation of one modality from another, including label prediction. We demonstrate these capabilities on both a synthetic dataset of noisy bidirectional spirals, as well as a real world dataset of labelled human actions. Our experiments show that our method learns and performs excellently on each of these tasks, while outperforming state-of-the-art inference methods that rely upon RNNs.

2 Methods

2.1 Multimodal Deep Markov Models

We introduce Multimodal Deep Markov Models (MDMMs) as a generalization of Krishnan *et al.*'s Deep Markov Models (DMMs) [9]. In a MDMM (Figure 1(a)), we model multiple sequences of observations, each of which is conditionally independent of the other sequences given the latent state variables. Each observation sequence corresponds to a particular data or sensor modality (e.g. video, audio, labels), and may be missing when other modalities are present. An MDMM can thus be seen as a sequential version of the MVAE [20].

Formally, let z_t and x_t^m respectively denote the latent state and observation for modality m at time t . An MDMM with M modalities is then defined by the transition and emission distributions:

$$z_t \sim \mathcal{N}(G_\alpha(z_{t-1}), S_\beta(z_{t-1})) \quad (\text{Transition}) \quad (1)$$

$$x_t^m \sim \Pi(F_{\kappa_m}(z_t)) \quad (\text{Emission for } m \in [1, M]) \quad (2)$$

Here, G_α , S_β and F_{κ_m} are functions (e.g., neural networks) which output the distribution parameters, and are themselves parameterized by α , β and κ_m respectively. We denote the model parameters by $\theta = \{\alpha, \beta, \kappa_1, \dots, \kappa_M\}$. We also use $z_{t_1:t_2}$ to denote the time-series of z from t_1 to t_2 , and $x_{t_1:t_2}^{m_1:m_2}$ to denote the corresponding observations from modalities m_1 to m_2 . We omit the modality superscripts when all modalities are present (i.e., $x_t \equiv x_t^{1:M}$).

As with VAEs [21] and MVAEs [20], we want to jointly learn the parameters θ, ϕ of the generative model $p_\theta(z_{1:T}, x_{1:T}) = p_\theta(x_{1:T}, z_{1:T})p_\theta(z_{1:T})$ and a variational posterior $q_\phi(z_{1:T}|x_{1:T})$ which approximates the true (intractable) posterior $p_\theta(z_{1:T}|x_{1:T})$. To do so, we maximize a lower bound on the log marginal likelihood $L(x; \theta, \phi) \leq p_\theta(x_{1:T})$, also known as the evidence lower bound (ELBO):

$$L(x; \theta, \phi) = \mathbb{E}_{q_\phi(z_{1:T}|x_{1:T})}[\log p_\theta(x_{1:T}|z_{1:T})] - \mathbb{E}_{q_\phi(z_{1:T}|x_{1:T})}[\text{KL}(q_\phi(z_{1:T}|x_{1:T})||p_\theta(z_{1:T}))] \quad (3)$$

In practice, we can maximize the ELBO with respect to θ and ϕ via gradient ascent with stochastic backpropagation [21, 22]. Doing so requires sampling from the variational posterior $q_\phi(z_{1:T}|x_{1:T})$. The computation of this posterior is what differentiates our method from many recent approaches to variational inference in time series models. In the following sections, we derive a variational posterior that factorizes over time-steps and modalities, allowing us to tractably infer the latent states $z_{1:T}$ even when data is missing.

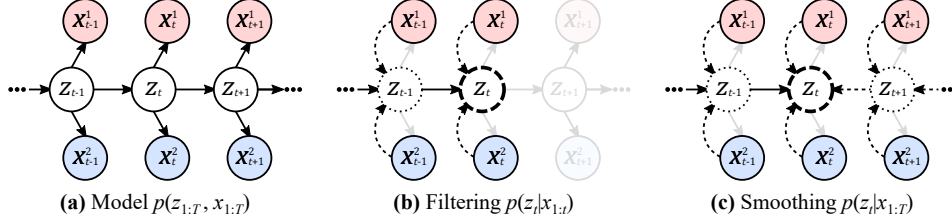


Figure 1: (a) A Multimodal Deep Markov Model (MDMM) with $M = 2$ modalities. Observations (filled) are generated from unobserved latent states (unfilled). (b) Filtering infers the current latent state z_t (bold dashed outline) given all observations up to t (solid outlines), and marginalizes (dotted outline) over past latent states. (c) Smoothing infers z_t given past, present, and future observations, and marginalizes over both past and future latent states.

2.2 Factorized Distributions for Filtering, Smoothing, and Sequencing

In latent sequence models such as MDMMs, we often want to perform several kinds of inferences over the latent states. The most common and important of such latent state inferences are:

Filtering	$p(z_t x_{1:t})$	Inferring the current z_t given all observations thus far.
Smoothing	$p(z_t x_{1:T})$	Inferring some z_t given all observations in the sequence $x_{1:T}$.
Sequencing	$p(z_{1:T} x_{1:T})$	Inferring the complete latent sequence $z_{1:T}$ from $x_{1:T}$.

Most architectures that combine deep learning with Markov models focus upon filtering [7, 5, 23, 24], while Krishnan *et al.* optimize their DMM for sequencing [9]. One of our contributions is to demonstrate that we can learn the filtering, smoothing, and sequencing distributions within the same framework, because they all share similar factorizations (see Figures 1(b) and 1(c) for the shared inference structure of filtering and smoothing). A further consequence of these factorizations is that we can naturally handle inferences given missing modalities or time-steps.

To demonstrate this similarity, we first factorize the sequencing distribution $p(z_{1:T} | x_{1:T})$ over time:

$$p(z_{1:T} | x_{1:T}) = p(z_1 | x_{1:T}) \prod_{t=2}^T p(z_t | z_{t-1}, x_{t:T}) \quad (4)$$

This factorization means that each latent state z_t depends only on the previous latent state z_{t-1} , as well as all current and future observations $x_{t:T}$, and is implied by the graphical structure of the MDMM (Figure 1(a)). We term $p(z_t | z_{t-1}, x_{t:T})$ the *conditional smoothing posterior*, because it is the posterior that corresponds to the *conditional prior* $p(z_t | z_{t-1})$ on the latent space, and because it combines information from the past and the future (hence ‘smoothing’).

Given one or more modalities, we can show that the conditional smoothing posterior $p(z_t | z_{t-1}, x_{t:T})$, the *backward* filtering distribution $p(z_t | x_{t:T})$, and the smoothing distribution $p(z_t | x_{1:T})$ all factorize almost identically:

$$p(z_t | x_{t:T}) \propto p(z_t | x_{t+1:T}) \left[\prod_{m=1}^M \frac{p(z_t | x_t^m)}{p(z_t)} \right] \quad (\text{Backward Filtering}) \quad (5)$$

$$p(z_t | x_{1:T}) \propto p(z_t | x_{t+1:T}) \left[\prod_{m=1}^M \frac{p(z_t | x_t^m)}{p(z_t)} \right] \frac{p(z_t | x_{1:t-1})}{p(z_t)} \quad (\text{Forward Smoothing}) \quad (6)$$

$$p(z_t | z_{t-1}, x_{t:T}) \propto p(z_t | x_{t+1:T}) \left[\prod_{m=1}^M \frac{p(z_t | x_t^m)}{p(z_t)} \right] \frac{p(z_t | z_{t-1})}{p(z_t)} \quad (\text{Cond. Smooth. Post.}) \quad (7)$$

Equations 5–7 show that each distribution can be decomposed into (i) its dependence on future observations, $p(z_t | x_{t+1:T})$, (ii) its dependence on each modality m in the present, $p(z_t | x_t^m)$, and, excluding filtering, (iii) its dependence on the past $p(z_t | z_{t-1})$ or $p(z_t | x_{1:t-1})$. Their shared structure is due to the conditional independence of $x_{t:T}$ given z_t from all prior observations or latent states.

Here we show only the derivation for Equation 7, because the others follow by either dropping z_{t-1} (Equation 5), or replacing z_{t-1} with $x_{1:t-1}$ (Equation 6):

$$\begin{aligned}
p(z_t|z_{t-1}, x_{t:T}^{1:M}) &= \frac{p(x_{t:T}^{1:M}|z_t, z_{t-1})p(z_t|z_{t-1})}{p(x_{t:T}^{1:M}|z_{t-1})} && \text{(Bayes' rule)} \\
&= \frac{p(x_{t+1:T}^{1:M}|z_t)p(x_t^{1:M}|z_t)p(z_t|z_{t-1})}{p(x_{t:T}^{1:M}|z_{t-1})} && (x_{t:T}^{1:M} \perp z_{t-1}|z_t) \\
&\propto p(x_{t+1:T}^{1:M}|z_t) \left[\prod_{m=1}^M p(x_t^m|z_t) \right] p(z_t|z_{t-1}) && (x_t^i \perp x_t^j|z_t) \\
&= \frac{p(z_t|x_{t+1:T}^{1:M})p(x_{t+1:T}^{1:M})}{p(z_t)} \left[\prod_{m=1}^M \frac{p(z_t|x_t^m)p(x_t^m)}{p(z_t)} \right] p(z_t|z_{t-1}) && \text{(Bayes' rule)} \\
&\propto p(z_t|x_{t+1:T}^{1:M}) \left[\prod_{m=1}^M \frac{p(z_t|x_t^m)}{p(z_t)} \right] \frac{p(z_t|z_{t-1})}{p(z_t)} && \text{(Proportionality)}
\end{aligned}$$

The factorizations in Equations 5–7 lead to several useful insights. First, they show that any missing modalities $\bar{m} \in [1, M]$ at time t can simply be left out of the product over modalities, leaving us with distributions that correctly conditioned on only the modalities $[1, M] \setminus \{\bar{m}\}$ that are present. Second, they suggest that we can compute all three distributions if we can approximate the dependence on the future, $q(z_t|x_{t+1:T}) \simeq p(z_t|x_{t+1:T})$, learn approximate posteriors $q(z_t|x_t^m) \simeq p(z_t|x_t^m)$ for each modality m , and know the model dynamics $p(z_t)$, $p(z_t|z_{t-1})$.

2.3 Multimodal Temporal Fusion via Product-of-Gaussians

However, there are a few obstacles to performing tractable computation of Equations 5–7. One obstacle is that it is not tractable to compute the product of generic probability distributions. To address this, we adopt the approach used for the MVAE [20], making the assumption that each term in Equations 5–7 is Gaussian. If each distribution is Gaussian, then their products or quotients are also Gaussian and can be computed in closed form. Since this result is well-known, we state it in the supplement (see [20] for a proof).

This Product-of-Gaussians approach has the added benefit that the output distribution is dominated by the input Gaussian terms with lower variance (higher precision), thereby fusing information in a way that gives more weight to higher-certainty inputs [25, 4]. This automatically balances the information provided by each modality m , depending on whether $p(z_t|x_t^m)$ is high or low certainty, as well as the information provided from the past and future through $p(z_t|z_{t-1})$ and $p(z_t|x_{t+1:T})$, thereby performing multimodal temporal fusion in a manner that is uncertainty-aware.

2.4 Approximate Backward Filtering with Missing Data

Another obstacle to computing Equations 5–7 is the dependence on future observations, $p(z_t|x_{t+1:T})$, which does not admit further factorization, and hence does not readily handle missing data among those future observations. Other approaches to approximating this dependence on the future rely on RNNs as recognition models [9, 16], but these are not designed to work with missing data.

To address this obstacle in a more principled manner, our insight was that $p(z_t|x_{t+1:T})$ is the expectation of $p(z_t|z_{t+1})$ under the backwards filtering distribution, $p(z_{t+1}|x_{t+1:T})$:

$$p(z_t|x_{t+1:T}) = \mathbb{E}_{p(z_{t+1}|x_{t+1:T})} [p(z_t|z_{t+1})] \quad (8)$$

For tractable approximation of this expectation, we use an approach similar to assumed density filtering [26]. We assume both $p(z_t|x_{t+1:T})$ and $p(z_t|z_{t+1})$ to be multivariate Gaussian with diagonal covariance, and sample the parameters μ, Σ of $p(z_t|z_{t+1})$ under $p(z_{t+1}|x_{t+1:T})$. After drawing K samples, we approximate the parameters of $p(z_t|x_{t+1:T})$ via empirical moment-matching:

$$\hat{\mu}_{z_t|x_{t+1:T}} = \frac{1}{K} \sum_{k=1}^K \mu_k \quad \hat{\Sigma}_{z_t|x_{t+1:T}} = \frac{1}{K} \sum_{k=1}^K (\Sigma_k + \mu_k^2) - \hat{\mu}_{z_t|x_{t+1:T}}^2 \quad (9)$$

Approximating $p(z_t|x_{t+1:T})$ by $p(z_t|z_{t+1})$ led us to three important insights. First, by substituting the expectation from Equation 8 into Equation 5, the backward filtering distribution becomes:

$$p(z_t|x_{t:T}) \propto \mathbb{E}_{p(z_{t+1}|x_{t+1:T})} [p(z_t|z_{t+1})] \left[\prod_{m=1}^M \frac{p(z_t|x_t^m)}{p(z_t)} \right] \quad (10)$$

In other words, by sampling under the filtering distribution for time $t + 1$, $p(z_{t+1}|x_{t+1:T})$, we can compute the filtering distribution for time t , $p(z_t|x_{t:T})$. We can thus recursively compute $p(z_t|x_{t:T})$ backwards in time, starting from time $t = T$.

Second, once we can perform filtering backwards in time, we can use this to approximate $p(z_t|x_{t+1:T})$ in the smoothing distribution (Equation 6) and the conditional smoothing posterior (Equation 7). Backward filtering hence allows approximation of both the smoothing and sequencing distributions.

Third, this approach removes the explicit dependence on all future observations $x_{t+1:T}$, allowing us to handle missing data. Suppose the data points $X_{\#} = \{x_{t_i}^{m_i}\}$ are missing, where t_i and m_i are the time-step and modality of the i th missing point respectively. Rather than directly compute the dependence on incomplete set of future observations, $p(z_t|x_{t+1:T} \setminus X_{\#})$, we can instead sample z_{t+1} under the filtering distribution conditioned on incomplete observations, $p(z_{t+1}|x_{t+1:T} \setminus X_{\#})$, and then compute $p(z_t|z_{t+1})$ given the sampled z_{t+1} , thereby approximating $p(z_t|x_{t+1:T} \setminus X_{\#})$.

2.5 Bidirectional Factorized Variational Inference

We now introduce factorized variational approximations of Equations 5–7. We replace the true posteriors $p(z_t|x_t^m)$ with approximations $q(z_t|x_t^m) = \tilde{q}(z_t|x_t^m)p(z_t)$, where $\tilde{q}(z_t|x_t^m)$ is parameterized by a (time-invariant) neural network for each modality m . Like [20], we directly learn the Gaussian quotients $\tilde{q}(z_t|x_t^m) = q(z_t|x_t^m)/p(z_t)$ to avoid the constraint required for ensuring a quotient of Gaussians is well-defined. We also parameterize the transition dynamics $p(z_t|z_{t-1})$ and $p(z_t|z_{t+1})$ using neural networks for the quotient distributions. This gives the following approximations:

$$q(z_t|x_{t:T}) \propto \mathbb{E}_{\leftarrow} [p(z_t|z_{t+1})] \prod_{m=1}^M \tilde{q}(z_t|x_t^m) \quad (\text{Backward Filtering}) \quad (11)$$

$$q(z_t|x_{1:T}) \propto \mathbb{E}_{\leftarrow} [p(z_t|z_{t+1})] \prod_{m=1}^M \tilde{q}(z_t|x_t^m) \frac{\mathbb{E}_{\rightarrow} [p(z_t|z_{t-1})]}{p(z_t)} \quad (\text{Forward Smoothing}) \quad (12)$$

$$q(z_t|z_{t-1}, x_{t:T}) \propto \mathbb{E}_{\leftarrow} [p(z_t|z_{t+1})] \prod_{m=1}^M \tilde{q}(z_t|x_t^m) \frac{p(z_t|z_{t-1})}{p(z_t)} \quad (\text{Cond. Smooth. Post.}) \quad (13)$$

Here, \mathbb{E}_{\leftarrow} is shorthand for the expectation under the approximate backward filtering distribution $q(z_{t+1}|x_{t+1:T})$, while \mathbb{E}_{\rightarrow} is the expectation under the forward smoothing distribution $q(z_{t-1}|x_{1:T})$.

To calculate the backward filtering distribution $q(z_t|x_{t:T})$, we introduce a *variational backward algorithm* (Algorithm 1) to recursively compute Equation 11 for all time-steps t in a single pass. Note that simply by reversing time in Algorithm 1, this gives us a *variational forward algorithm* that computes the forward filtering distribution $q(z_t|x_{1:t})$.

Unlike filtering, smoothing and sequencing require information from both the past ($p(z_t|z_{t-1})$) and the future ($p(z_t|z_{t+1})$). This motivates a *variational backward-forward algorithm* (Algorithm 2) for smoothing and sequencing. Algorithm 2 first uses Algorithm 1 as a backward pass, then performs a forward pass to propagate information from past to future.¹

While Algorithm 1 approximates the filtering distribution $q(z_t|x_{t:T})$, by setting the number of particles $K = 1$, it effectively computes the (backward) conditional filtering posterior $q(z_t|z_{t+1}, x_t)$ and (backward) conditional prior $p(z_t|z_{t+1})$ for a randomly sampled latent sequence $z_{1:T}$. Similarly, while Algorithm 2 approximates smoothing by default, when $K_f = 1$, it effectively computes the

¹Algorithm 2 also requires knowing $p(z_t)$ for each t . While this can be computed through sampling in the forward pass, we choose to avoid the instability by instead assuming $p(z_t)$ is constant with time, i.e., the MDMM is stationary when no observations are given. During training, we add $\text{KL}(p(z_t) || \mathbb{E}_{z_{t-1}} p(z_t|z_{t-1}))$ and $\text{KL}(p(z_t) || \mathbb{E}_{z_{t+1}} p(z_t|z_{t+1}))$ to the loss to ensure that the transition dynamics obey this assumption.

Algorithm 1 A variational backward algorithm for approximate backward filtering.

```

function BACKWARDFILTER( $x_{1:T}, K$ )
  Initialize  $q(z_t|x_{T+1:T}) \leftarrow p(z_T)$ 
  for  $t = T$  to 1 do
    Let  $\mathcal{M} \subseteq [1, M]$  be the observed modalities at  $t$ 
     $q(z_t|x_{t:T}) \leftarrow q(z_t|x_{t+1:T}) \prod_{m \in \mathcal{M}} \tilde{q}(z_t|x_t^m)$ 
    Sample  $K$  particles  $z_t^k \sim q(z_t|x_{t:T})$  for  $k \in [1, K]$ 
    Compute  $p(z_{t-1}|z_t^k)$  for each particle  $z_t^k$ 
     $q(z_{t-1}|x_{t:T}) \leftarrow \frac{1}{K} \sum_{k=1}^K p(z_{t-1}|z_t^k)$ 
  end for
  return  $\{q(z_t|x_{t:T}), q(z_t|x_{t+1:T}) \text{ for } t \in [1, T]\}$ 
end function

```

Algorithm 2 A variational backward-forward algorithm for approximate forward smoothing.

```

function FORWARDSMOOTH( $x_{1:T}, K_b, K_f$ )
  Initialize  $\tilde{p}(z_t|x_{1:0}) \leftarrow 1$ 
  Collect  $q(z_t|x_{t+1:T})$  from output of BACKWARDFILTER( $x_{1:T}, K_b$ )
  for  $t = 1$  to  $T$  do
    Let  $\mathcal{M} \subseteq [1, M]$  be the observed modalities at  $t$ 
     $q(z_t|x_{1:T}) \leftarrow q(z_t|x_{t+1:T}) \prod_{m \in \mathcal{M}} [\tilde{q}(z_t|x_t^m)] q(z_t|x_{1:t-1}) / p(z_t)$ 
    Sample  $K_f$  particles  $z_t \sim q(z_t|x_{1:T})$  for  $k \in [1, K_f]$ 
    Compute  $p(z_{t+1}|z_t^k)$  for each particle  $z_t^k$ 
     $q(z_{t+1}|x_{1:t}) \leftarrow \frac{1}{K_f} \sum_{k=1}^{K_f} p(z_{t+1}|z_t^k)$ 
  end for
  return  $\{q(z_t|x_{1:T}), q(z_t|x_{1:t-1}) \text{ for } t \in [1, T]\}$ 
end function

```

(forward) conditional smoothing posterior $q(z_t|z_{t-1}, x_{t:T})$ and (forward) conditional prior $p(z_t|z_{t-1})$ for a random latent sequence $z_{1:T}$. These quantities are useful not only because they allow us to perform sequencing, but also because we can use them to compute the ELBO for both backward filtering and forward smoothing:

$$L_{\text{filter}} = \sum_{t=1}^T \left[\mathbb{E}_{q(z_t|x_{t:T})} \log p(x_t|z_t) - \mathbb{E}_{q(z_{t+1}|x_{t+1:T})} \text{KL}(q(z_t|z_{t+1}, x_t) || p(z_t|z_{t+1})) \right] \quad (14)$$

$$L_{\text{smooth}} = \sum_{t=1}^T \left[\mathbb{E}_{q(z_t|x_{1:T})} \log p(x_t|z_t) - \mathbb{E}_{q(z_{t-1}|x_{1:T})} \text{KL}(q(z_t|z_{t-1}, x_{t:T}) || p(z_t|z_{t-1})) \right] \quad (15)$$

L_{filter} is the filtering ELBO because it corresponds to a 'backward filtering' variational posterior $q(z_{1:T}|x_{1:T}) = \prod_t q(z_t|z_{t+1}, x_t)$, where each z_t is only inferred using the current observation x_t and the future latent state z_{t+1} . L_{smooth} is the smoothing ELBO because it corresponds to the correct factorization of the posterior in Equation 4, where each term combines information from both past and future. Because we require accurate backward filtering in order to perform forward smoothing, we learn the MDMM parameters θ, ϕ by jointly maximizing the filtering and smoothing ELBOs. We call this paradigm **bidirectional factorized variational inference (BFVI)**, due to its use of factorized variational posteriors for both backward filtering and forward smoothing.

3 Experiments

We compare **BFVI** against state-of-the-art RNN-based inference methods on two multimodal time series datasets over a range of inference tasks. **F-Mask** and **F-Skip** use forward RNNs (one per modality), using zero-masking and update skipping respectively to handle missing data. They are thus multimodal variants of the ST-L network in [9], and similar to the variational RNN [5] and recurrent SSM [23]. **B-Mask** and **B-Skip** use backward RNNs, with masking and skipping respectively, and correspond to the Deep Kalman Smoother in [9]. The underlying MDMM architecture is constant across inference methods. Architectural and training details can be found in the supplement.

3.1 Datasets

Noisy Spirals. We synthesized a dataset of 1000 noisy 2D spirals (600 train / 400 test) similar to Chen *et al.* [15], treating the x and y coordinates as two separate modalities. Spiral trajectories vary in direction (clockwise or counter-clockwise), size, and aspect ratio, and Gaussian noise is added to the observations. We used 5 latent dimensions, and two-layer perceptrons for encoding $q(z_t|x_t^m)$ and decoding $p(x_t^m|z_t)$. For evaluation, we compute the mean squared error (MSE) per time step between the predicted trajectories and ground truth spirals.

Weizmann Human Actions. This is a video dataset of 9 people each performing 10 actions [27]. We converted it to a trimodal time series dataset by treating actions and people’s identities as per-frame labels, similar to He *et al.* [28]. Each RGB frame was cropped to the central 128×128 window and resized to 64×64 . We selected one person’s videos as the test set, and the other 80 videos as the training set, allowing us to test action label prediction on an unseen person. We used 256 latent dimensions, and convolutional / deconvolutional neural networks for encoding and decoding. For evaluation, we compute the Structural Similarity (SSIM) between the input video frames and the reconstructed outputs.

3.2 Tasks

We evaluated all methods on the following suite of temporal inference tasks for both datasets:

<i>Reconstruction</i>	Reconstruction given complete observations
<i>Drop Half</i>	Reconstruction after half of the inputs are randomly deleted.
<i>Forward Extrapolation</i>	Predicting the last 25% of a sequence when the rest is given.
<i>Backward Extrapolation</i>	Inferring the first 25% of a sequence when the rest is given.

When evaluating the above tasks on the Weizmann dataset, we provided only video frames as input, to test whether the methods were capable of unimodal inference after multimodal training. We also tested cross-modal inference using the following **conditional generation / label prediction** tasks:

<i>Cond. Gen. (Spirals)</i>	Given x - and initial 25% of y -coordinates, generate rest of spiral.
<i>Cond. Gen. (Video)</i>	Given action and identity labels & first 25% of frames, generate rest of video.
<i>Label Pred. (Video)</i>	Infer the action labels for each frame, given only the video frames.

3.3 Results

Method	Recon.	Drop Half	Fwd. Extra.	Bwd. Extra.	Cond. Gen.	Label Pred.
Spirals Dataset: MSE (SD)						
BFVI	0.02 (0.01)	0.04 (0.01)	0.12 (0.10)	0.07 (0.03)	0.26 (0.26)	–
F-Mask	0.02 (0.01)	0.06 (0.02)	0.10 (0.08)	0.18 (0.07)	1.37 (1.39)	–
F-Skip	0.04 (0.01)	0.10 (0.05)	0.13 (0.11)	0.19 (0.06)	1.51 (1.54)	–
B-Mask	0.02 (0.01)	0.04 (0.01)	0.18 (0.14)	0.04 (0.01)	1.25 (1.23)	–
B-Skip	0.05 (0.01)	0.19 (0.05)	0.32 (0.22)	0.37 (0.15)	1.64 (1.51)	–
Weizmann Video Dataset: SSIM or Accuracy* (SD)						
BFVI	.83 (.04)	.82 (.04)	.83 (.04)	.81 (.05)	.81 (.03)	.66 (.34)*
F-Mask	.78 (.04)	.70 (.17)	.78 (.04)	.66 (.18)	.78 (.04)	.19 (.21)*
F-Skip	.71 (.16)	.70 (.17)	.71 (.16)	.67 (.18)	.71 (.16)	.24 (.39)*
B-Mask	.67 (.20)	.76 (.11)	.67 (.19)	.53 (.24)	.68 (.20)	.40 (.43)*
B-Skip	.79 (.04)	.78 (.03)	.79 (.04)	.78 (.03)	.79 (.04)	.18 (.30)*

Table 1: Evaluation metrics on both datasets across inference methods and tasks. Best performance per task (column) in bold. (Top) *Spirals Dataset*: MSE (lower is better) per time-step between reconstructions and ground truth spirals. For scale, the average squared spiral radius is about 5 sq. units. (Bottom) *Weizmann Video Dataset*: SSIM or label accuracy (higher is better) per time-step with respect to original videos. Means and Standard Deviations (SD) are across the test set.

We present the results of the inference methods in Table 1, and show sample reconstruction results for spirals in Figures 2 and videos in Figure 3. On the spirals dataset, BFVI achieves high performance on all tasks, whereas the RNN-based methods only perform well on a few. In particular, all methods besides BFVI do poorly on the conditional generation task, which can be understood from the right-most column of Figure 2. BFVI generates a spiral that matches the provided x -coordinates, while the next-best method, B-Mask, completes the trajectory with a plausible spiral, but ignores the x observations entirely in the process.

On the more complex Weizmann video dataset, BFVI outperforms all other methods on every task, demonstrating both the power and flexibility of our approach. The RNN-based methods performed especially poorly on label prediction, and this was the case even on the training set (not shown in Table 1). We suspect this occurred because they lack a principled approach to multimodal fusion, and hence fail to learn a latent space which captures the mutual information between action labels and images. In contrast, BFVI learns to both predict one modality from another, and to propagate information across time, as can be seen from the reconstruction and predictions in Figure 3.

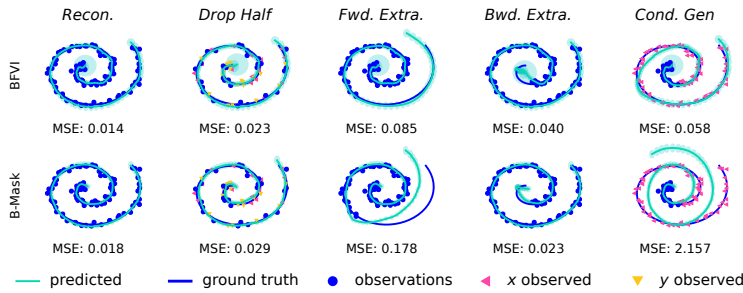


Figure 2: Reconstructions for all 5 spiral inference tasks for BFVI and the next best method, B-Mask. BFVI outperforms B-Mask significantly on both forward extrapolation and conditional generation.

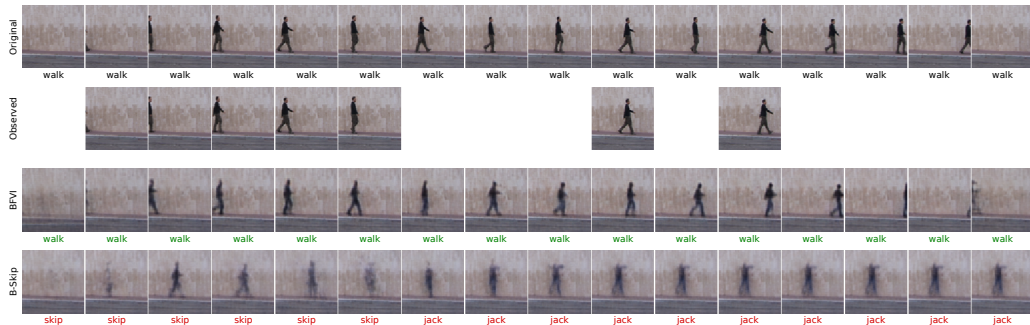


Figure 3: Reconstructions of a ‘walking’ video from the test set (1st row), with half of the frames deleted at random, the last 25% removed, and no action labels provided (2nd row). Despite never having seen the person in the video, BFVI reconstructs a walking silhouette, and also correctly predicts the action (3rd row). By contrast, B-Skip (the next best method) wrongly predicts the action label, and vacillates between different possible action silhouettes over time (4th row).

4 Conclusion

In this paper, we introduced bidirectional factorized variational inference (BFVI) as a novel inference method for Multimodal Deep Markov Models. This method handles incomplete data via a factorized variational posterior, allowing us to easily marginalize over missing observations. Our method is thus capable of a large range of multimodal temporal inference tasks, which we demonstrate on both a synthetic dataset and a video dataset of human motions. The ability to handle missing data also suggests applications in weakly supervised learning of labelled time series [20], as well as modelling of multi-rate time series [16]. Given the abundance of multimodal time series data where missing data is the norm rather than the exception, our work holds great promise for many future applications.

References

- [1] Rudolph Emil Kalman. A new approach to linear filtering and prediction problems. *Journal of basic Engineering*, 82(1):35–45, 1960.
- [2] Anca D Dragan, Kenton CT Lee, and Siddhartha S Srinivasa. Legibility and predictability of robot motion. In *Proceedings of the 8th ACM/IEEE international conference on Human-robot interaction*, pages 301–308. IEEE Press, 2013.
- [3] Chris L Baker, Julian Jara-Ettinger, Rebecca Saxe, and Joshua B Tenenbaum. Rational quantitative attribution of beliefs, desires and percepts in human mentalizing. *Nature Human Behaviour*, 1(4):0064, 2017.
- [4] Desmond C Ong, Jamil Zaki, and Noah D Goodman. Affective cognition: Exploring lay theories of emotion. *Cognition*, 143:141–162, 2015.
- [5] Junyoung Chung, Kyle Kastner, Laurent Dinh, Kratarth Goel, Aaron C Courville, and Yoshua Bengio. A recurrent latent variable model for sequential data. In *Advances in neural information processing systems*, pages 2980–2988, 2015.
- [6] Justin Bayer and Christian Osendorfer. Learning stochastic recurrent networks. In *NIPS 2014 Workshop on Advances in Variational Inference*, 2014.
- [7] Otto Fabius and Joost R van Amersfoort. Variational recurrent auto-encoders. *arXiv preprint arXiv:1412.6581*, 2014.
- [8] Marco Fraccaro, Søren Kaae Sønderby, Ulrich Paquet, and Ole Winther. Sequential neural models with stochastic layers. In *Advances in Neural Information Processing Systems*, pages 2199–2207, 2016.
- [9] Rahul G Krishnan, Uri Shalit, and David Sontag. Structured inference networks for nonlinear state space models. In *Thirty-First AAAI Conference on Artificial Intelligence*, 2017.
- [10] Evan Archer, Il Memming Park, Lars Buesing, John Cunningham, and Liam Paninski. Black box variational inference for state space models. *arXiv preprint arXiv:1511.07367*, 2015.
- [11] Matthew Johnson, David K Duvenaud, Alex Wiltschko, Ryan P Adams, and Sandeep R Datta. Composing graphical models with neural networks for structured representations and fast inference. In *Advances in Neural Information Processing Systems*, pages 2946–2954, 2016.
- [12] Maximilian Karl, Maximilian Soelch, Justin Bayer, and Patrick van der Smagt. Deep variational bayes filters: Unsupervised learning of state space models from raw data. *arXiv preprint arXiv:1605.06432*, 2016.
- [13] Andreas Doerr, Christian Daniel, Martin Schiegg, Nguyen-Tuong Duy, Stefan Schaal, Marc Toussaint, and Trimpe Sebastian. Probabilistic recurrent state-space models. In Jennifer Dy and Andreas Krause, editors, *Proceedings of the 35th International Conference on Machine Learning*, volume 80 of *Proceedings of Machine Learning Research*, pages 1280–1289, Stockholmsmässan, Stockholm Sweden, 10–15 Jul 2018. PMLR.
- [14] Wu Lin, Mohammad Emtiyaz Khan, and Nicolas Hubacher. Variational message passing with structured inference networks. In *International Conference on Learning Representations*, 2018.
- [15] Tian Qi Chen, Yulia Rubanova, Jesse Bettencourt, and David K Duvenaud. Neural ordinary differential equations. In *Advances in Neural Information Processing Systems*, pages 6571–6583, 2018.
- [16] Zhengping Che, Sanjay Purushotham, Guangyu Li, Bo Jiang, and Yan Liu. Hierarchical deep generative models for multi-rate multivariate time series. In Jennifer Dy and Andreas Krause, editors, *Proceedings of the 35th International Conference on Machine Learning*, volume 80 of *Proceedings of Machine Learning Research*, pages 784–793, Stockholmsmässan, Stockholm Sweden, 10–15 Jul 2018. PMLR.
- [17] Zachary C Lipton, David Kale, and Randall Wetzel. Directly modeling missing data in sequences with rnns: Improved classification of clinical time series. In *Machine Learning for Healthcare Conference*, pages 253–270, 2016.
- [18] Daniel Neil, Michael Pfeiffer, and Shih-Chii Liu. Phased lstm: Accelerating recurrent network training for long or event-based sequences. In *Advances in neural information processing systems*, pages 3882–3890, 2016.

- [19] Marco Fraccaro, Simon Kamronn, Ulrich Paquet, and Ole Winther. A disentangled recognition and nonlinear dynamics model for unsupervised learning. In *Advances in Neural Information Processing Systems*, pages 3601–3610, 2017.
- [20] Mike Wu and Noah Goodman. Multimodal generative models for scalable weakly-supervised learning. In *Advances in Neural Information Processing Systems*, pages 5575–5585, 2018.
- [21] Diederik P Kingma and Max Welling. Auto-encoding variational bayes. In *International Conference on Learning Representations*, 2014.
- [22] Danilo Jimenez Rezende, Shakir Mohamed, and Daan Wierstra. Stochastic backpropagation and approximate inference in deep generative models. In *International Conference on Machine Learning*, pages 1278–1286, 2014.
- [23] Danijar Hafner, Timothy Lillicrap, Ian Fischer, Ruben Villegas, David Ha, Honglak Lee, and James Davidson. Learning latent dynamics for planning from pixels. *arXiv preprint arXiv:1811.04551*, 2018.
- [24] Lars Buesing, Theophane Weber, Sebastien Racaniere, SM Eslami, Danilo Rezende, David P Reichert, Fabio Viola, Frederic Besse, Karol Gregor, Demis Hassabis, et al. Learning and querying fast generative models for reinforcement learning. *arXiv preprint arXiv:1802.03006*, 2018.
- [25] Yanshuai Cao and David J Fleet. Generalized product of experts for automatic and principled fusion of gaussian process predictions. In *Modern Nonparametrics 3: Automating the Learning Pipeline Workshop, NeurIPS 2014.*, 2014.
- [26] Marco F Huber, Frederik Beutler, and Uwe D Hanebeck. Semi-analytic gaussian assumed density filter. In *Proceedings of the 2011 American Control Conference*, pages 3006–3011. IEEE, 2011.
- [27] Lena Gorelick, Moshe Blank, Eli Shechtman, Michal Irani, and Ronen Basri. Actions as space-time shapes. *IEEE transactions on pattern analysis and machine intelligence*, 29(12):2247–2253, 2007.
- [28] Jiawei He, Andreas Lehrmann, Joseph Marino, Greg Mori, and Leonid Sigal. Probabilistic video generation using holistic attribute control. In *Proceedings of the European Conference on Computer Vision (ECCV)*, pages 452–467, 2018.

Supplemental Material

Factorized Inference in Deep Markov Models for Incomplete Multimodal Time Series

Zhi-Xuan Tan¹, Harold Soh², Desmond C. Ong¹

¹A*STAR AI Initiative, Agency for Science, Technology and Research, Singapore

²Department of Computer Science, National University of Singapore

xuan@mit.edu, harold@comp.nus.edu.sg, desmond.c.ong@gmail.com

A Products and Quotients of Gaussian Distributions

Here we state the closed form solution for the quotient of two products a finite number of Gaussian distributions. We define:

$$g(x) = \prod_{i=1}^k f(x|\mu_i, \Sigma_i) \Big/ \prod_{j=k+1}^l f(x|\mu_j, \Sigma_j),$$

where each $f(x|\mu_i, \Sigma_i)$ is a multivariate Gaussian with mean μ_i , covariance Σ_i and precision $T_i = \Sigma_i^{-1}$. Under the constraint that $\sum_{i=1}^k T_i > \sum_{j=k+1}^l T_j$ element-wise, $g(x)$ is also multivariate Gaussian with mean and covariance:

$$\mu_g = \frac{\sum_{i=1}^k \mu_i T_i - \sum_{j=k+1}^l \mu_j T_j}{\sum_{i=1}^k T_i - \sum_{j=k+1}^l T_j} \quad \Sigma_g = \left(\sum_{i=1}^k T_i - \sum_{j=k+1}^l T_j \right)^{-1}$$

If the constraint is not satisfied, then $g(x)$ cannot be normalized into a well-defined probability distribution. The reader may refer to [1] for a modern proof.

B Multimodal Bidirectional Training Loss

Bidirectional factorized variational inference (BFVI) requires training the Multimodal Deep Markov Model (MDMM) to perform both backward filtering and forward smoothing. In addition, the model has to learn how to perform inference given multiple modalities, both jointly and in isolation. As such, we extend the multimodal training paradigm proposed for the MVAE [1]. For each batch of training data, we compute and minimize the following multimodal bidirectional training loss:

$$L = \lambda_{\text{filter}} \left[L_{\text{filter}}^{1:M} + \sum_{m=1}^M L_{\text{filter}}^m \right] + \lambda_{\text{smooth}} \left[L_{\text{smooth}}^{1:M} + \sum_{m=1}^M L_{\text{smooth}}^m \right] + \lambda_{\text{match}} L_{\text{match}}$$

Here, λ_{filter} , λ_{smooth} and λ_{match} are loss multipliers. $L_{\text{filter}}^{1:M}$ and $L_{\text{smooth}}^{1:M}$ are the multimodal ELBO losses for filtering and smoothing respectively:

$$L_{\text{filter}}^{1:M} = \sum_{t=1}^T \left[\mathbb{E}_{q(z_t|x_{t:T}^{1:M})} \sum_{m=1}^M \lambda_m \log p(x_t^m | z_t) - \mathbb{E}_{q(z_{t+1}|x_{t+1:T}^{1:M})} \beta \text{KL} \left(q(z_t | z_{t+1}, x_t^{1:M}) \parallel p(z_t | z_{t+1}) \right) \right]$$

$$L_{\text{smooth}}^{1:M} = \sum_{t=1}^T \left[\mathbb{E}_{q(z_t|x_{1:T}^{1:M})} \sum_{m=1}^M \lambda_m \log p(x_t^m | z_t) - \mathbb{E}_{q(z_{t-1}|x_{1:t}^{1:M})} \beta \text{KL} \left(q(z_t | z_{t-1}, x_t^{1:M}) \parallel p(z_t | z_{t-1}) \right) \right]$$

λ_m is the reconstruction loss multiplier for modality m , and β is the loss multiplier for the KL divergence. L_{filter}^m and L_{smooth}^m are the corresponding unimodal ELBO losses:

$$L_{\text{filter}}^m = \sum_{t=1}^T \left[\mathbb{E}_{q(z_t|x_{1:T}^m)} \lambda_m \log p(x_t^m|z_t) - \mathbb{E}_{q(z_{t+1}|x_{1:T}^m)} \beta \text{KL} \left(q(z_t|z_{t+1}, x_t^m) \parallel p(z_t|z_{t+1}) \right) \right]$$

$$L_{\text{smooth}}^m = \sum_{t=1}^T \left[\mathbb{E}_{q(z_t|x_{1:T}^m)} \lambda_m \log p(x_t^m|z_t) - \mathbb{E}_{q(z_{t-1}|x_{1:T}^m)} \beta \text{KL} \left(q(z_t|z_{t-1}, x_t^m) \parallel p(z_t|z_{t-1}) \right) \right]$$

L_{match} is the prior matching loss, to ensure that the forward and backward dynamics conform the assumption that $p(z_t)$ is invariant with t :

$$L_{\text{match}} = \text{KL} \left(p(z_t) \parallel \mathbb{E}_{z_{t-1}} p(z_t|z_{t-1}) \right) + \text{KL} \left(p(z_t) \parallel \mathbb{E}_{z_{t+1}} p(z_t|z_{t+1}) \right)$$

To compute L_{match} , we need to sample particles from $p(z_t)$, introducing K_p , the number of prior matching particles, as a hyper-parameter. Similarly, we need to perform backward filtering with sampling to compute the smoothing ELBOs, for which we use K_b backward filtering particles.

C Model and Inference Architectures

C.1 Transition Functions

We use a variant of the Gated Transition Function (GTF) from [2] to parameterize both the forward transition $p(z_t|z_{t-1})$ and backward transition $p(z_t|z_{t+1})$:

$$g_t = \text{Sigmoid} \circ \text{Linear}_{|z| \leftarrow |h|} \circ \text{ReLU} \circ \text{Linear}_{|h| \leftarrow |z|}(z_t)$$

$$\tilde{\mu}_t = \text{Linear}_{|z| \leftarrow |h|} \circ \text{ReLU} \circ \text{Linear}_{|h| \leftarrow |z|}(z_t)$$

$$\bar{\mu}_t = \text{Linear}_{|z| \leftarrow |z|}(z_t)$$

$$\mu_t = g_t \odot \tilde{\mu}_t + (1 - g_t) \odot \bar{\mu}_t$$

$$\sigma_t = \text{Softplus} \circ \text{Linear}_{|z| \leftarrow |z|}(\tilde{\mu}_t)$$

where $\text{Linear}_{b \leftarrow a}$ is a linear mapping from a to b dimensions, \circ is function composition, and \odot is element-wise multiplication, $|z|$ is the dimension of the latent space (5 for spirals, 256 for videos), and $|h|$ is the dimension of the hidden layer (20 for spirals, 256 for videos). To stabilize training when using BFVI, we found it necessary to add a small constant (0.001) to the standard deviation, σ_t . To be clear, we learn separate networks each for the forward and backward transitions.

C.2 Encoders and Decoders

For the spirals dataset, we use multi-layer perceptrons as encoders and decoders from and to the x and y coordinates. Let v be a place-holder for either x or y , and recall that for the encoder, we learn a network that parameterizes the quotient $\tilde{q}(z_t|v_t) = q(z_t|v_t)/p(z_t)$. The architectures are:

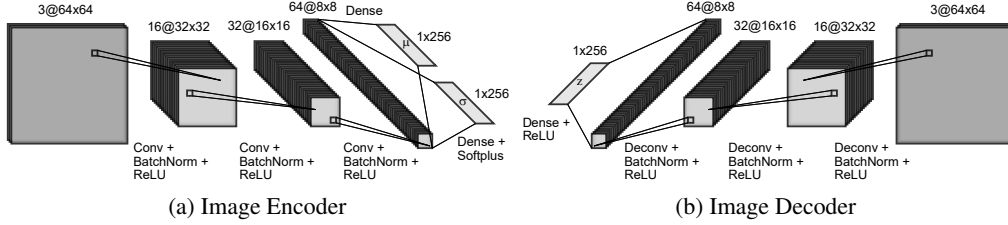
$$\begin{aligned} \tilde{q}(z_t|v_t) &\sim \mathcal{N}(\mu_z, \sigma_z) & p(v_t|z_t) &\sim \mathcal{N}(\mu_v, \sigma_v) \\ h &= \text{ReLU} \circ \text{Linear}_{|h| \leftarrow |z|}(v_t) & h &= \text{ReLU} \circ \text{Linear}_{|h| \leftarrow |z|}(z_t) \\ \mu_z &= \text{Linear}_{|z| \leftarrow |h|}(h) & \mu_v &= \text{Linear}_{1 \leftarrow |h|}(h) \\ \sigma_z &= \text{Softplus} \circ \text{Linear}_{|z| \leftarrow |h|}(h) & \sigma_v &= \text{Softplus} \circ \text{Linear}_{1 \leftarrow |h|}(h) \end{aligned}$$

where we used $|h| = 20$.

For the Weizmann video dataset, we used a variant of the above encoders and decoders to work with categorical distributions over the action and person labels. Again we use v as a placeholder. The architectures are:

$$\begin{aligned} \tilde{q}(z_t|v_t) &\sim \mathcal{N}(\mu_z, \sigma_z) & p(v_t|z_t) &\sim \text{Categorical}(p_1, \dots, p_k) \\ e &= \text{ReLU} \circ \text{Embedding}_{|h|}(v_t) & h &= \text{ReLU} \circ \text{Linear}_{|h| \leftarrow |z|}(z_t) \\ h &= \text{ReLU} \circ \text{Linear}_{|h| \leftarrow |h|}(e) & (p_1, \dots, p_k) &= \text{Softmax} \circ \text{Linear}_{k \leftarrow |h|}(h) \\ \mu_z &= \text{Linear}_{|z| \leftarrow |h|}(h) \\ \sigma_z &= \text{Softplus} \circ \text{Linear}_{|z| \leftarrow |h|}(h) \end{aligned}$$

The number of categories is denoted by k (10 for actions, 9 for people), and we used $|h| = 256$. For the encoders and decoders from and to images (video frames), see Supplementary Figure 1 below.



Supplementary Figure 1: Image encoder and decoder architectures. Convolutional layers use 3×3 kernels, de-convolutional layers use 4×4 kernels, both use a stride of 2 and padding of 1.

C.3 Inference Networks

The encoder architectures described in the previous section are designed to work with BFVI, and so they directly output distribution parameters μ_z, σ_z for the latent state z_t . To adapt them to work with the RNN-based structured inference networks (F-Mask, F-Skip, B-Mask, B-Skip), we simply remove the Gaussian output layers from each encoder, using the features f_t^m of the penultimate layer as inputs to the RNN at each time step.

We follow the original DMM implementation [2] in using Gated Recurrent Units (GRUs) for the structured inference networks. To generalize this to the multimodal case, we have one GRU per modality, which we label GRU_m for modality m . The difference between the Mask and Skip methods is that the former uses zero-masking of missing inputs:

$$h_{t\pm 1}^m = \begin{cases} \text{GRU}_m(f_t^m, h_t^m) & \text{if } x_t^m \text{ is present} \\ \text{GRU}_m(0, h_t^m) & \text{otherwise} \end{cases}$$

whereas the latter skips the update for the hidden state h_t^m of GRU_m whenever x_t^m is missing:

$$h_{t\pm 1}^m = \begin{cases} \text{GRU}_m(f_t^m, h_t^m) & \text{if } x_t^m \text{ is present} \\ h_t^m & \text{otherwise} \end{cases}$$

Update skipping is the method used in [2]’s implementation to handle missing data. For the forward RNNs (F-Mask and F-Skip), we take the positive sign in the plus-minus signs above, while for the backward RNNs (B-Mask and B-Skip), we take the negative sign.

In order to combine the information from the RNNs with the previous latent state z_{t-1} to infer the current latent state z_t , we use a variant of the combiner function from [2] that takes in z_{t-1} and the hidden states h_t^m of all modalities as inputs:

$$\begin{aligned} \tilde{q}(z_t | z_{t-1}, x_{1:T}) &\sim \mathcal{N}(\mu_z, \sigma_z) \\ h &= \text{ReLU} \circ \text{Linear}_{|h| \leftarrow |z_{t-1}|} (z_{t-1}, h_t^1, \dots, h_t^M) \\ \mu_z &= \text{Linear}_{|z| \leftarrow |h|} (h) \\ \sigma_z &= \text{Softplus} \circ \text{Linear}_{|z| \leftarrow |h|} (h) \end{aligned}$$

We use $|h| = 5$ for the spirals dataset and $|h| = 256$ for the videos (same dimensions for the both the hidden layer and the GRU hidden states). Because the above formulation has no direct connection from the current input x_t to the current latent state z_t , it seemed like it would hurt performance when we needed z_t to be a good low-dimensional representation of x_t . As such, for the video dataset, we used a variant that also takes in the encoded features f_t^m as inputs (if x_t^m is missing, then the corresponding feature f_t^m is zero-masked):

$$\begin{aligned} \tilde{q}(z_t | z_{t-1}, x_{1:T}) &\sim \mathcal{N}(\mu_z, \sigma_z) \\ h &= \text{ReLU} \circ \text{Linear}_{|h| \leftarrow |z_{t-1}|} (z_{t-1}, h_t^1, \dots, h_t^M, f_t^1, \dots, f_t^M) \\ \mu_z &= \text{Linear}_{|z| \leftarrow |h|} (h) \\ \sigma_z &= \text{Softplus} \circ \text{Linear}_{|z| \leftarrow |h|} (h) \end{aligned}$$

Table 1 compares the number of neural network parameters (model networks + inference networks) required for BFVI vs. the RNN-based inference methods. Despite matching hidden layer dimensions, BFVI still uses 2 to 3 times less parameters, because it does not require inference RNNs for each modality, and uses Product-of-Gaussians for fusion instead of a combiner network.

Method	Number of parameters	
	<i>Spirals</i>	<i>Weizmann</i>
BFVI	1854	4542503
RNN-based	7124	7494183

Table 1: Number of network parameters for each method.

D Training Parameters

Parameter		Spirals	Weizmann
Filtering ELBO mult.	λ_{filter}	0.5	''
Smoothing ELBO mult.	λ_{smooth}	0.5	''
Prior matching mult.	λ_{match}	0.01 β	''
Reconstruction mult.	λ_m	$x, y: 1$	Vid.: 1, Act.:10, Pers.: 10
KL divergence mult.	β	Anneal(0,1) over E_β	''
Bwd. filtering particles	K_b	25	''
Prior matching particles	K_p	50	''
Training epochs	E	500	3000
β -annealing epochs	E_β	100	1500
Early stopping		Yes	Yes
Batch size		100	50
Sequence splitting		No	Into 25 time-step segments
Optimizer		ADAM	''
Learning rate		0.02 (BFVI), 0.01 (Rest)	5×10^{-4}
Weight decay		1×10^{-4}	
Burst deletion rate		0.1	0.2

Table 2: Training parameters for spirals and Weizmann datasets.

Table 2 provides the training parameters we used. Unless specified, parameters were kept constant across inference methods. As in most VAE-like models, we anneal β , the multiplier for the KL divergence loss from 0 to 1 over time. This incentivizes the model to first find encoders and decoders that reconstruct well, before regularizing the latent space [3]. Since the prior matching multiplier λ_{match} also serves to regularize the latent space, we tie its value to β , so that it increases as β increases.

To speed up training on the video dataset, we split each input sequence into segments that were 25 time steps long, and trained on those segments. To improve the robustness to missing data when training each methods, we also introduced burst deletion errors — random contiguous deletions of inputs. For the spirals dataset, we deleted input segments at training time that were 0.1 long as the original video lengths. For the video dataset, we deleted input segments at training time that were 0.2 long as the original video lengths. Deletion start points were selected uniformly at random.

We briefly discuss training differences between BFVI and other methods here. For the RNN-based methods, no bidirectional training is involved, so we only minimized the (forward) filtering ELBO (for F-Mask, F-Skip) or the smoothing ELBO (for B-Mask, B-Skip). While we also tried to use the multimodal training paradigm (i.e. minimizing the sum of $L^{1:M}$ and L^m) for the RNN-based methods, the effects of this were mixed: On the spirals dataset, performance dropped very sharply with the multimodal paradigm, whereas performance increased on the Weizmann video dataset. As such, the results we report in the main manuscript use the multimodal training paradigm only for the video dataset. For the spirals dataset, we only minimize $L^{1:M}$, with all inputs provided, but not L^m , which is computed with only modality m provided as input. Finally, we used a higher learning rate (0.02) for BFVI on the spirals dataset because we noticed slow convergence with the lower rate of 0.01. Increasing the learning rate to 0.02 for the other methods hurt their performance.

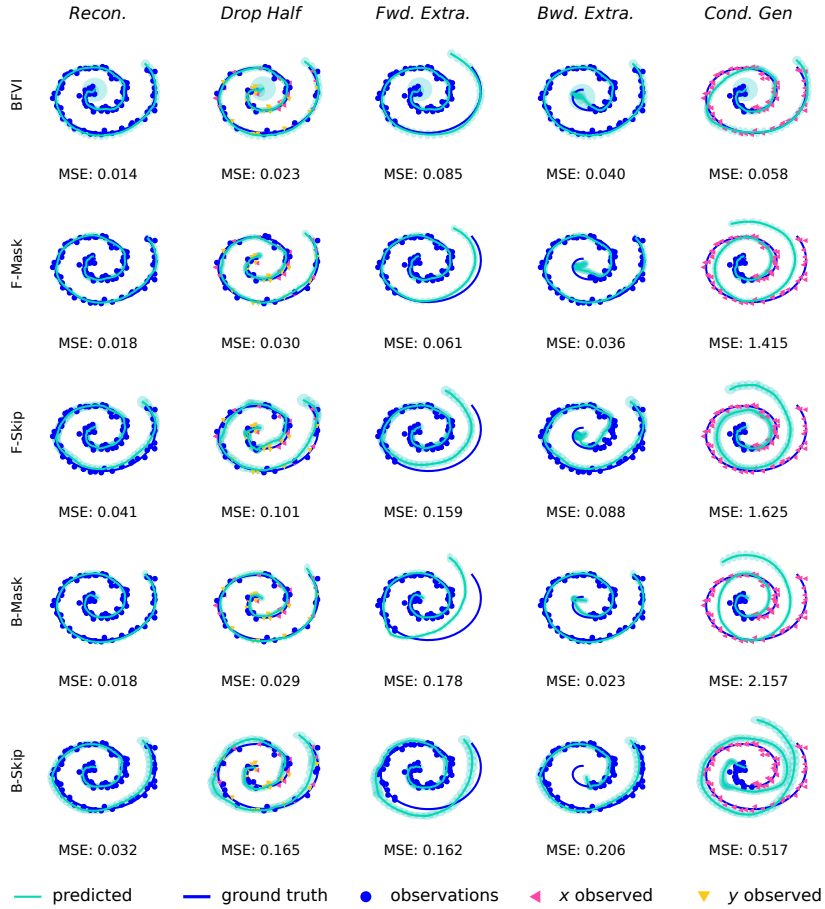
E Evaluation Details

When evaluating the models, we estimate the MAP latent sequence $z_{1:T}^* = \arg \max_{z_{1:T}} p(z_{1:T} | x_{1:T})$ by estimating $\hat{z}_t = \arg \max_{z_{1:T}} q(z_t | \hat{z}_{t-1}, x_{1:T})$ for each t (i.e., we recursively take the mean of the approximate conditional smoothing posterior, $q(z_t | \hat{z}_{t-1}, x_{1:T})$.) For reconstruction, we then decode this inferred latent sequence and take the MLE of the observations, $\hat{x}_{1:T} = \arg \max_{x_{1:T}} p(x_{1:T} | \hat{z}_{1:T})$. While this does not infer the exact MAP sequence, it has been standard practice for recurrent latent variable models [2], and we find it empirically adequate in lieu of approximate Viterbi sequencing.

In the case of BFVI, we also have to specify number of filtering particles K_b for the backward pass at evaluation time. We used $K_b = 200$ for additional stability, though we found that lower values also produced similar results.

F Additional Results

To supplement the reconstruction figures in the main paper which only compared BFVI to the next-best-performing method, here we show a more complete comparison on the Spirals dataset (Supplementary Figure 2).

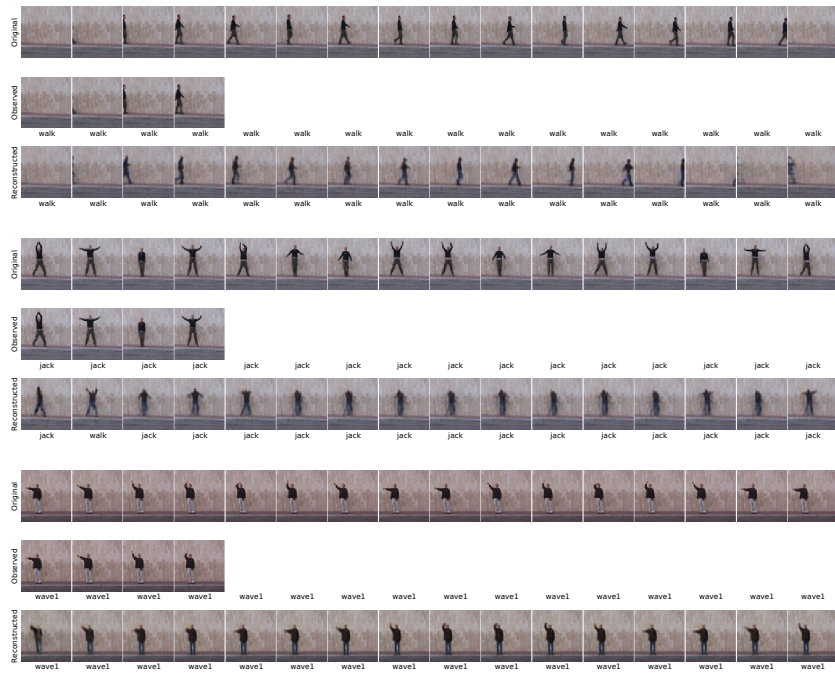


Supplementary Figure 2: Reconstructions for all 5 spiral inference tasks (columns) for all methods (rows). Our BFVI method does well on all tasks, but especially better than the other methods on the Conditioned Generation task (right-most column), where only the x - and first 25% of the y -coordinates are given.

To demonstrate that our method can generate realistic videos of human actions given only action labels and initial video segments, we show the results for conditional generation via BFVI in Supplementary Figures 3 and 4. The initial segments used in Figure 4 are from the test set, showing our method’s ability to generalize to unseen data. Initial segments are the first 25% of the source videos.



Supplementary Figure 3: Conditional generation of video from labels on the training set.



Supplementary Figure 4: Conditional generation of video from labels on the test set.

References

- [1] Mike Wu and Noah Goodman. Multimodal generative models for scalable weakly-supervised learning. In *Advances in Neural Information Processing Systems*, pages 5575–5585, 2018.
- [2] Rahul G Krishnan, Uri Shalit, and David Sontag. Structured inference networks for nonlinear state space models. In *Thirty-First AAAI Conference on Artificial Intelligence*, 2017.
- [3] Samuel R Bowman, Luke Vilnis, Oriol Vinyals, Andrew M Dai, Rafal Jozefowicz, and Samy Bengio. Generating sentences from a continuous space. *arXiv preprint arXiv:1511.06349*, 2015.